TECHNICAL ARTICLE

Study on the Thermal Expansion Behavior of Mg-3RE Alloys and Mg-3Y/SiC$_p$ Composites

TONG WANG [1,2,7] CAN WANG,[1,2] CHAOQI FENG,[3] RUIZHEN GUO,[1,2] WENYI HU,[4] DABIAO XIA,[5] QICHI LE,[1,2] and MANOJ GUPTA[6]

1.—The Key Laboratory of Electromagnetic Processing of Materials, Ministry of Education, Northeastern University, Shenyang 110819, China. 2.—School of Materials Science and Engineering, Northeastern University, Shenyang 110819, China. 3.—Institute of Metal Research, Chinese Academy of Sciences, Shenyang 110016, China. 4.—Department of Chemistry and Materials, Longyan University, Longyan 364012, China. 5.—Jihua Laboratory, Foshan 528000, China. 6.—College of Design and Engineering, National University of Singapore, Singapore 117575, Singapore. 7.—e-mail: wangtong@epm.neu.edu.cn

The high coefficient of thermal expansion (CTE) of magnesium alloys leads to poor thermal dimensional stability and limits its application in the electronic field. This work focused on understanding the effect of rare earth (RE) on the thermal expansion behavior of Mg and attempted to tailor the CTE with SiC particulates. Composites were manufactured by gravity casting with ultrasonic dispersion treatment. The effect of 3 wt.% RE (Sm, Nd, Gd, Y) on the microstructure and thermal expansion behavior of the Mg alloys was explored. Adding RE can lead to the formation of RE-containing second phases and marginally decreased the CTE of magnesium. The CTEs of Mg-3Sm, Mg-3Nd, Mg-3Gd and Mg-3Y alloys were 27.3×10^{-6}/°C, 27.0×10^{-6}/°C, 27.2×10^{-6}/°C and 27.8×10^{-6}/°C, respectively. The influence of SiC$_p$ on the thermal expansion behavior of Mg-3Y was also investigated. The SiC$_p$ promoted the precipitation of Mg$_{24}$Y$_5$ phase in the extruded Mg-3Y/SiC$_p$ composites and significantly reduced the CTE. The CTEs of Mg/3SiC, Mg-3Y/1SiC, Mg-3Y/3SiC and Mg-3Y/5SiC were 27.4×10^{-6}/°C, 26.8×10^{-6}/°C, 26.6×10^{-6}/°C and 23.3×10^{-6}/°C, respectively. Rule of mixture, the Turner model and the Kerner model were utilized to predict the CTE of the Mg-3Y/xSiC$_p$ (x = 1, 3, 5) composites. The predictions of the Kerner model show a better correlation with the experimental results.

INTRODUCTION

Magnesium alloys have the advantages of low density, high specific strength, excellent thermal conductivity and exceptional electromagnetic interference (EMI) shielding properties.[1] In recent years, they have been increasingly used in electronic industries, such as making computer shells, heat sink components, etc.[2] The coefficient of thermal expansion (CTE) of α-magnesium is as high as 27.0×10^{-6}/°C, while that of aluminum and copper is about 23.3×10^{-6}/°C and 17.4×10^{-6}/°C, respectively.[3–5] Due to the heat generated by electronic circuits, thermal expansion will occur and leads to a mismatch between Mg alloy components and the connecting parts of aluminum and copper alloys. It has an adverse effect on the accuracy and service life of the components and limits the application of Mg alloys in the electronic field. Therefore, it is of great importance to develop magnesium alloys with good thermal stability, i.e., low CTE. However, there is very limited research on the thermal expansion behavior of magnesium alloys.

The thermal expansion coefficient of the alloy is mostly determined by its phase composition. Gupta et al.[6] reported that adding copper as reinforcement marginally reduced the CTE of pure magnesium because of the presence of Mg$_2$Cu phase. Wu et al.[7] reported that the CTE of Mg-4Si was as low as

$17.98 \times 10^{-6}/°C$ due to the formation of the Mg$_2$Si phase. However, Mg$_2$Si is a brittle phase, too much of which will deteriorate the mechanical properties of the alloy significantly.[8] Adding Ca could further decrease the CTE of Mg-4Si because of the formation of CaMgSi phase. Nobuhiro et al.[9] investigated the thermal expansion of a 18R-synchronized long period stacking ordered (LPSO) magnesium alloy Mg$_{85}$Zn$_6$Y$_9$ in the temperature range of − 178–167 °C. Its CTE was only $18.53 \times 10^{-6}/°C$. However, this kind of LPSO magnesium alloy was not very common and normally requires special manufacturing techniques. Rahulan et al.[10] found that the CTE of the Mg-Li alloys was particularly dependent on the content of Li. The CTE of β phase was higher than that of α phase. Thus, with an increasing amount of Li, more β phase would form and lead to the higher CTE. However, this kind of phase transformation only existed in the Mg-Li series alloys.

Rare earths (REs) are important alloying elements in magnesium alloys, which can significantly improve the high-temperature mechanical properties. Besides, the CTEs of REs are much lower than for Mg.[11] For example, the CTEs of Ce and Nd are as low as $6.7 \times 10^{-6}/°C$ and $12.1 \times 10^{-6}/°C$, respectively.[12] Kumar et al.[13] reported that the CTE of the Mg-3Al-xLa (x = 0, 1, 2.5, 4 wt.%) alloys decreased with alloying additions of Al and the increasing concentration of La. It was attributed to the low CTEs of Al and La, which are $23.1 \times 10^{-6}/°C$ and $12.1 \times 10^{-6}/°C$, respectively. Ma et al.[14] pointed out that the CTE of the Mg-1Al-xY (x = 4, 6, 8 wt.%) alloys decreased with the increasing content of Y due to the precipitation of the Al$_2$Y phase. Dong et al.[15] found the CTE of Mg-2Nd and Mg-4Nd were $22.71 \times 10^{-6}/°C$ and $18.57 \times 10^{-6}/°C$, respectively, owing to the precipitation of Mg$_{41}$Nd$_5$. Even though RE can decrease the CTE of Mg alloys, the conventional alloying method has reached a certain limit in further decreasing it.[3]

The CTE of silicon carbide particulates (SiC$_p$) is as low as $7.75 \times 10^{-6}/°C$. There are some studies on the Mg alloy-based composites reinforced with SiC$_p$ prepared with different techniques.[16–22] Jayamathy et al.[23] reported that the CTE of die cast AZ92 alloy, AZ92/SiC (10 vol.%) and AZ92/SiC (15 vol.%) composites were about $26 \times 10^{-6}/°C$, $21.53 \times 10^{-6}/°C$ and $19.79 \times 10^{-6}/°C$, respectively. Wong et al.[24] revealed a 14% reduction in the average CTE values of the magnesium matrix with the addition of hybrid length scales (micro + nano) of SiC reinforcement manufactured by powder metallurgy. Thakur et al.[25] investigated the thermal expansion behavior of magnesium-based hybrid composites containing nano-sized SiC$_p$ and carbon nanotube (CNT) reinforcements fabricated through powder metallurgy technique. The addition of SiC and CNT reinforcements lowered the CTE value of the magnesium matrix. It was attributed to much lower CTE of the dispersed nano-particles. Moreover, SiC nano-particles appeared to have a superior ability to constrain the matrix expansion compared to CNT. Hong et al.[26] measured and calculated the CTE of liquid pressed AZ91 magnesium alloy matrix composites reinforced with SiC$_p$. The predicted CTE of AZ91/SiC$_p$ with the Kerner's model was in good agreement with the experimental result.

Up to now, there has been no systematic study on the effect of RE elements on the thermal expansion behavior of magnesium alloys or the effect of SiC$_p$ on the thermal expansion behavior of Mg-RE alloy-based composites fabricated through gravity casting method. Moreover, the combined role of second phases and SiC particulates on the thermal expansion behavior of magnesium alloy-based composites is still unclear. In this work, the commonly used alloying RE elements in Mg of Sm, Nd, Gd and Y were selected to make four Mg-3RE binary alloys. In addition, different composites of Mg/3SiCp and Mg-3Y/xSiC$_p$ (x = 1, 3 and 5 wt.%) composites were prepared using the gravity casting method with ultrasonic dispersion treatment. The effects of adding SiC$_p$ and the amount of SiC$_p$ on the thermal expansion behavior of the Mg-3Y alloy-based composites were investigated. Finally, the three models of the rule of mixture, the Turner model and the Kerner model were utilized to predict the CTE of the Mg-3Y/SiC$_p$ composites and compared. The present study provides guidance for designing and developing magnesium alloy-based composites with controllable CTE.

MATERIALS AND EXPERIMENTAL METHODS

Preparation of the Materials

The Mg-3Sm, Mg-3Nd, Mg-3Gd and Mg-3Y alloys were prepared using pure Mg ingots (99.95% purity) and the Mg-25wt.%RE master alloys (Baotou Research Institute of Rare Earths, China). The amount of the master alloy used was calculated using the smelting yield of 70%, 73%, 90% and 65% for Mg-25%Sm, Mg-25%Nd, Mg-25%Gd and Mg-25%Y, respectively. A mixture of 99 vol.% CO$_2$ and 1 vol.% SF$_6$ gas was utilized throughout the whole casting process to prevent oxidation. First, the temperature of the smelting furnace was set at 750°C to melt the pure Mg ingots. Subsequently the temperature was decreased to 730°C and the oxidized slag was removed. Mg-RE master alloys were then added and melt was held for 5 min. The melt was then stirred for 5 min, added to the RJ-5 flux and kept for 15 min for refining. When the temperature further decreased to 710°C, the melt was poured into the casting mold which was preheated to 200°C. Pure Mg was prepared using the same method as the benchmark. The main composition of the RJ-5 flux is displayed in Table I.

For the preparation of the Mg-3Y/xSiC$_p$ (x = 1, 3 and 5 wt.%) composites, pure Mg ingots, the Mg-25wt.%Y master alloy and the SiC particulates with a diameter of 10 μm were utilized. A mixture of 99

Table I. Main composition of the RJ-5 flux (wt.%)

$MgCl_2$	KCl	$BaCl_2$	CaF_2	$CaCl_2$	NaCl	MgO	H_2O
26 ± 3	22 ± 3	29 ± 3	14 ± 3	4 ± 3	4 ± 3	1	0.5

vol% CO_2 and 1 vol.% SF_6 gas was used throughout the whole casting process to prevent oxidation. The melting furnace was preheated to 750°C to melt pure Mg ingots. When the melt was heated to 750°C, Mg-25%Y master alloy was added, and the melt was stirred. The temperature then was raised to 780°C, added the RJ-5 flux, stirred and held for 15 min for refining. The temperature was subsequently decreased to 720°C and SiC particulates were added. The composite slurry was stirred for 5 min and held for 20 min while an ultrasonic treatment was applied on the melt to disperse the SiC particulates. The frequency of the ultrasonic was 20 kHz and the power was 1500 W. After the ultrasonic treatment, the melt was heated to 780°C and poured into the mold preheated to 200°C.

For homogenization of the alloy and the composite ingots, they were heated in the box furnace in air to 520°C, held for 12 h and then air cooled. Even though there was little oxidization at the surface during the homogenization, the ingots were cut from Φ60 mm to Φ46 mm for extrusion. The extrusion was conducted at 300°C at a speed of 0.8 mm/s. The diameter of the extruded bars was Φ12 mm and the extrusion ratio was about 14.7.

Characterization

The observation of microstructure was performed on the longitudinal cross-section of the extruded alloy and composite bars. The specimens were ground using SiC papers of grit size 600, 800, 1200 and 2000 and then mechanical polished with diamond paste of 1.0 μm and 0.5 μm, respectively. To reveal the grains, etching was conducted with a solution of 10 ml water, 4.2 g picric acid, 10 ml glacial acetic acid and 70 ml alcohol.

For the phase composition, Thermal-Calc 2023a software with the TCMG6 database was used to predict the second phases in the four Mg-3RE alloys. Besides, a Rigaku SmartLab (9 kW) x-ray diffractometer (XRD) with Cu-Kα radiation was utilized to determine the second phases and the results were analyzed with the JADE software. The XRD specimens were ground using SiC papers of grit size 600, 800, 1200 and 2000.

The fraction of second phases, the distribution and fraction of SiC_p were analyzed on a Zeiss Ultra Plus scanning electron microscope (SEM) with an energy-dispersive spectrometer (EDS) at an acceleration voltage of 20 kV. The volume fraction of the second phases and the SiC_p reinforcements were analyzed using ImageJ-Pro software. The images for the calculation of the volume fraction of the second phases and the SiCp reinforcements were taken at the magnification of × 500. Three areas were used for each specimen and the average value of the volume fraction calculated.

The linear thermal expansion behavior of the extruded alloys and composites was determined along the extrusion direction (ED) with a high-temperature dilatometry equipment (NETZSCH DIL 402EP). For the heating process, the testing temperature range was 30–400°C at a heating rate of 5°C/min. For the cooling process, the testing temperature range was 400–50°C at a cooling rate of 3°C/min. The specimen dimension was Φ5 mm × 25 mm.

RESULTS

Microstructure and Thermal Expansion Behavior of the Mg-3RE Alloys

Figure 1 shows the optical microstructure of the four Mg-3RE alloys. The ED is along the vertical direction. The extruded alloys of Mg-3Sm, Mg-3Nd, Mg-3Gd and Mg-3Y showed a fully recrystallized microstructure with similar grain size of about 3.6 ± 0.1 μm, 2.7 ± 0.1 μm, 3.3 ± 0.1 μm and 3.8 ± 0.1 μm, respectively. Some second phases can be observed distributed along the ED.

The predicted composition of the second phases and the XRD spectra of the four alloys are displayed in Fig. 2a and b, respectively. It was determined that the second phases in the Mg-3Sm, Mg-3Nd, Mg-3Gd and Mg-3Y alloys were $Mg_{41}Sm_5$, $Mg_{41}Nd_5$, Mg_5Gd and $Mg_{24}Y_5$, respectively. Since second phases are a crucial factor affecting the thermal expansion performance of alloys, SEM analysis was conducted to further obtain the fraction of second phases in these alloys as shown in Fig. 3. The volume percents of the second phases in the Mg-3Sm, Mg-3Nd, Mg-3Gd and Mg-3Y alloys were 0.7%, 6.9%, 0.06% and 0.07%, respectively. This difference in the fraction of the second phases was because of the different solid solubility of these RE elements in magnesium, which will be discussed in more detail in the discussion part.

Figure 4 shows the thermal expansion curves and corresponding CTE curves of the Mg-3Sm, Mg-3Nd, Mg-3Gd and Mg-3Y specimens. For these four alloys, the relative length expansions (dL/L_0) increase with increasing temperature. The coefficient of thermal expansion (α), which is defined as the fractional change in length per unit change in temperature[27], can be expressed with the following equation[27]:
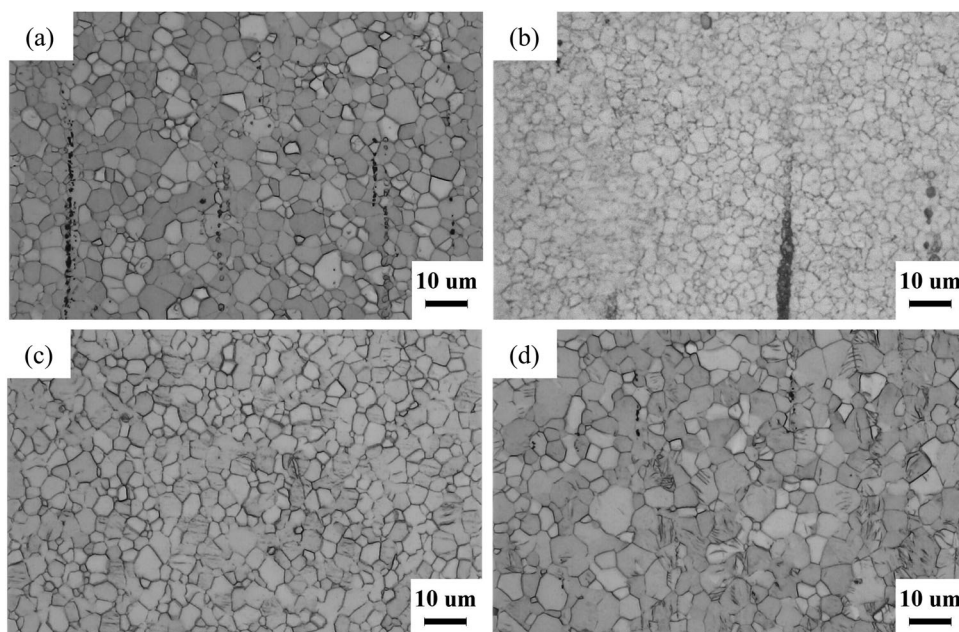
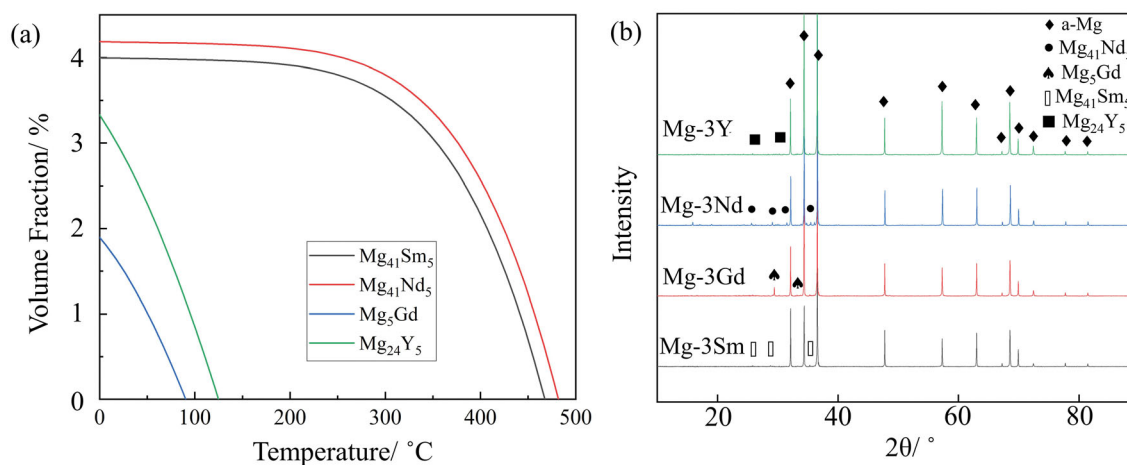Fig. 1. Optical microstructure of (a) Mg-3Sm, (b) Mg-3Nd, (c) Mg-3Gd and (d) Mg-3Y.

Fig. 2. (a) Calculated second phases and (b) XRD spectra of the Mg-3Y, Mg-3Nd, Mg-3Gd and Mg-3Sm alloys.

$$\alpha = \frac{\Delta L}{L_0 \times \Delta T} \qquad (1)$$

where L_0 was the initial length of the specimen, ΔL is the thermal expansion increment of the specimen, and ΔT was the increase of testing temperature.

According to Fig. 4, the CTE value increased rapidly at the early heating stage. When the temperature reached about 100°C, the increase of CTE became slow, which was related to the mismatch of CTE between the matrix and the second phases and the non-harmonic vibration of atoms.[4] The linear CTE α of the extruded Mg-3Sm, Mg-3Nd, Mg-3Gd and Mg-3Y specimens along the ED is listed in Table II. The CTE of pure Mg was also measured as a benchmark and shown together. Compared with pure Mg, the CTEs of the Mg-3RE

alloys were marginally lower. It indicates that adding RE elements slightly reduced the CTE of Mg. Among these four alloys, the Mg-3Nd alloy demonstrated the lowest CTE of 27.0×10^{-6}/°C. According to Section "Microstructure and Thermal Expansion Behavior of the Mg-3RE Alloys," RE-containing second phases formed in these Mg-3RE alloys. These second phases usually have good thermal stability and low CTE. Therefore, when the temperature started to rise and the Mg-3RE alloys began to expand, the different thermal expansion behavior between the second phases and the matrix would hinder the thermal expansion of the matrix and lower the CTE compared with pure Mg.
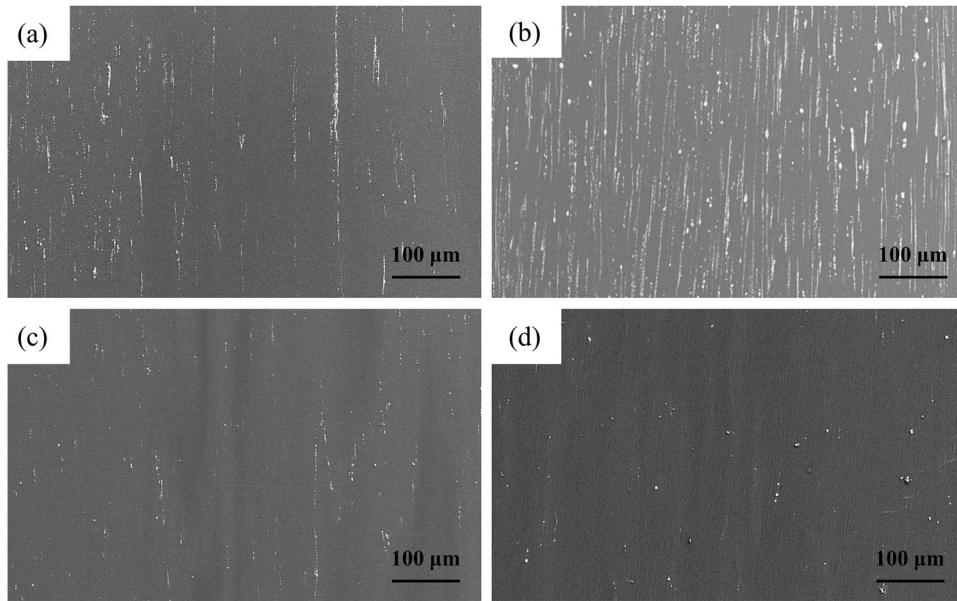
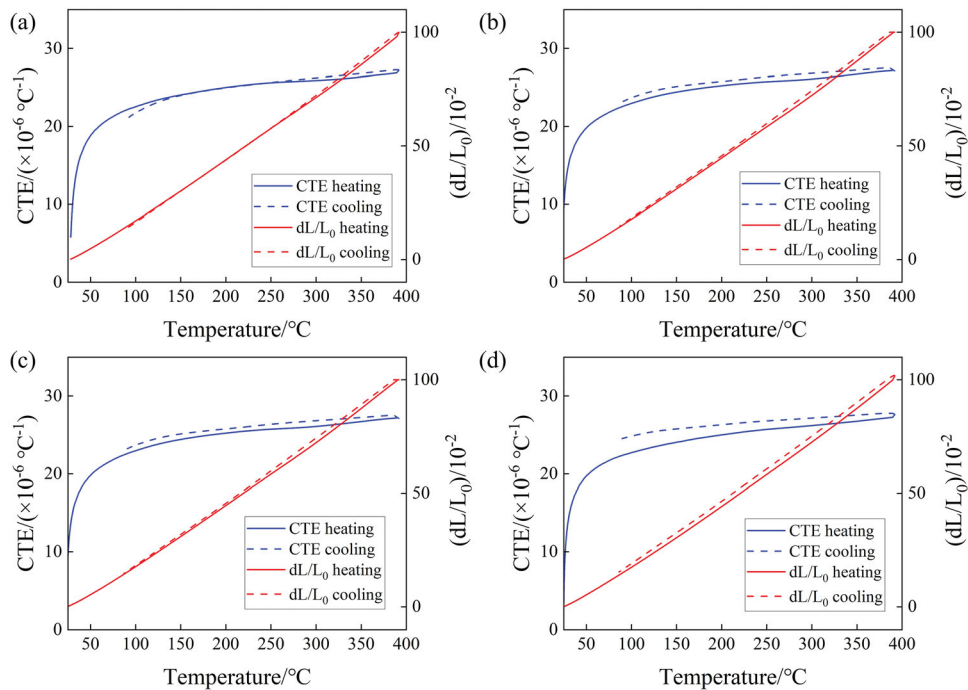Fig. 3. Secondary electron SEM microstructure of (a) Mg-3Sm, (b) Mg-3Nd, (c) Mg-3Gd and (d) Mg-3Y.

Fig. 4. Thermal expansion curves (red line) and experimental CTE curves (blue line) of (a) Mg-3Sm, (b) Mg-3Nd, (c) Mg-3Gd and (d) Mg-3Y.

Table II. Volume percent of second phases and the CTE α of the Mg-3RE alloys and pure Mg

Material	Volume percent of second phases (%)	α ($\times 10^{-6}$/°C)
Mg-3Sm	0.7	27.3
Mg-3Nd	6.9	27.0
Mg-3Gd	0.06	27.2
Mg-3Y	0.07	27.8
Pure Mg	–	27.9

Microstructure and Thermal Expansion Behavior of the SiC$_p$ Reinforced Composites

According to the above results, among the four Mg-3RE alloys, Mg-3Y demonstrated the highest CTE of $27.8 \times 10^{-6}/°C$. Therefore, in this part, different amounts of SiC particulates (1, 3 and 5 wt.%) were added to Mg-3Y as the matrix to investigate the effect of the SiC particulates on the microstructure and thermal expansion behavior of the Mg-3Y alloy. To provide a benchmark without the interference of second phase, 3 wt.% SiC particulates were also added to pure Mg to prepare the Mg/3SiC$_p$ composite.

Figure 5 displays the SEM and EDS mapping of two positions of the Mg/3SiC$_p$ composite showing the distribution and volume fraction of the SiC particulates, which had a significant impact on the thermal expansion coefficient of composites. The ED of the specimen was placed vertically. Since element Si only existed in the SiC particulates, the distribution of Si element in the EDS mapping reflected that of the SiC particulates. Even though ultrasonic treatment was conducted during the casting process of the composites, the distribution of the SiC particulates in the matrix was not uniform and some agglomeration occurred. Most SiC particulates aligned along the ED, which would lead to the asymmetric CTE values of the extruded composites transverse to or along the ED. To better calculate the fraction of the SiC particulates, two representative positions were selected to observe for each specimen as shown in Fig. 5a and b. In these two figures, the volume fractions of the SiC particulates were calculated to be about 3.2% and 2.6%, respectively, leading to an average volume fraction of SiC$_p$ of 2.9% in the Mg/3SiC$_p$ specimen. It meant even though the distribution of the SiC particulates was not quite uniform, most of them were still in the metal matrix. The same method of measuring the volume fraction of the SiC particulates was applied in the investigation of the Mg-3Y/xSiC$_p$ (x = 1, 3 and 5 wt.%) composites. However, for the sake of saving space, only the image of one representative position is shown for each specimen.

The SEM images and EDS mappings of the Mg-3Y/1SiC$_p$, Mg-3Y/3SiC$_p$ and Mg-3Y/5SiC$_p$ composites are shown in Fig. 6. In the Mg-3Y/1SiC$_p$ specimen, the distribution of the SiC particulates was relatively uniform along the ED. With the increasing number of SiC particulates, the agglomeration of the SiC particulates became more severe. The distributions of the SiC particulates in the Mg-3Y/3SiC$_p$ and Mg-3Y/5SiC$_p$ specimens were similar to those in Mg/3SiC$_p$ in Fig. 5. Moreover, the second phase and the SiC particulates distributed together in strips along the ED of the Mg-3Y/xSiC$_p$ composites. The volume percent of the SiC particulates and the second phase in the composites were calculated and are listed in Table III.

Since Si only existed in the SiC particulates and Y concentrated in the Mg$_{24}$Y$_5$ second phase, the distribution of elements Si and Y in the EDS mapping reflected those of the SiC particulates and the Mg$_{24}$Y$_5$ second phase. According to Table III, in the Mg-3Y/1SiC$_p$, Mg-3Y/3SiC$_p$ and Mg-3Y/5SiC$_p$ composites, the volume fractions of the SiC particulates were about 1.3%, 1.85% and 4.1%, respectively, and those of the Mg$_{24}$Y$_5$ second phase were about 1.62%, 1.73% and 2.22%, respectively (the uncertainties of measurements are 0.01%). The amount of the Mg$_{24}$Y$_5$ increased with the increasing number of the SiC particulates in the composites. As mentioned in Section "Microstructure and Thermal Expansion Behavior of the Mg-3RE Alloys," there was about 0.07% Mg$_{24}$Y$_5$ phase in the Mg-3Y alloy. Therefore, the addition of the SiC particulates promoted the precipitation of the Mg$_{24}$Y$_5$ second phase in the extruded Mg-3Y alloy.
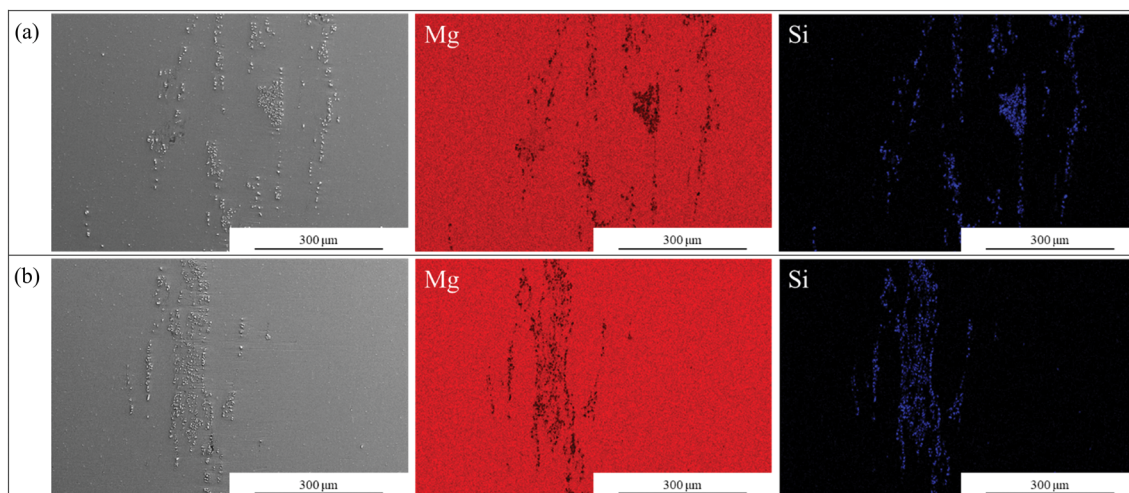

Fig. 5. SEM image and EDS mapping of Mg/3SiC$_p$: (a) region I and (b) region II.
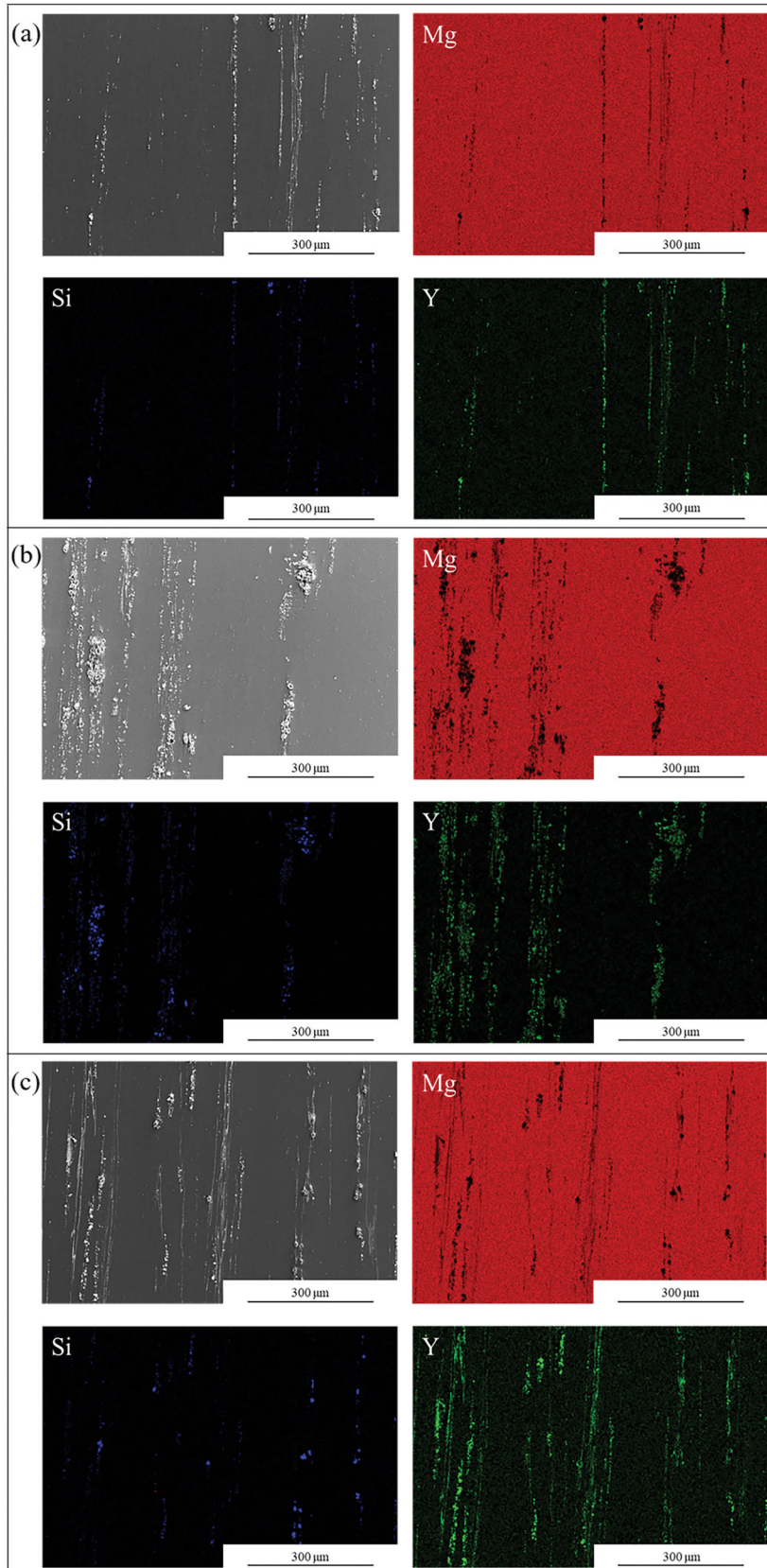
Fig. 6. SEM image and EDS mapping of (a) Mg-3Y/1SiC$_p$, (b) Mg-3Y/3SiC$_p$ and (c) Mg-3Y/5SiC$_p$.

Table III. Volume percent of SiC$_p$ and second phase in the SiC$_p$ reinforced composites and their corresponding CTE α values

Composite	SiC$_p$ (%)			Second phase (%)			α ($\times 10^{-6}$/°C)
	Region I	Region II	Average	Region I	Region II	Average	
Mg/3SiC	3.20	2.60	2.90	–	–	–	27.4
Mg-3Y/1SiC	1.40	1.20	1.30	1.27	1.96	1.62	26.8
Mg-3Y/3SiC	2.60	1.10	1.85	1.30	2.16	1.73	26.6
Mg-3Y/5SiC	4.00	4.20	4.10	1.90	2.54	2.22	23.3
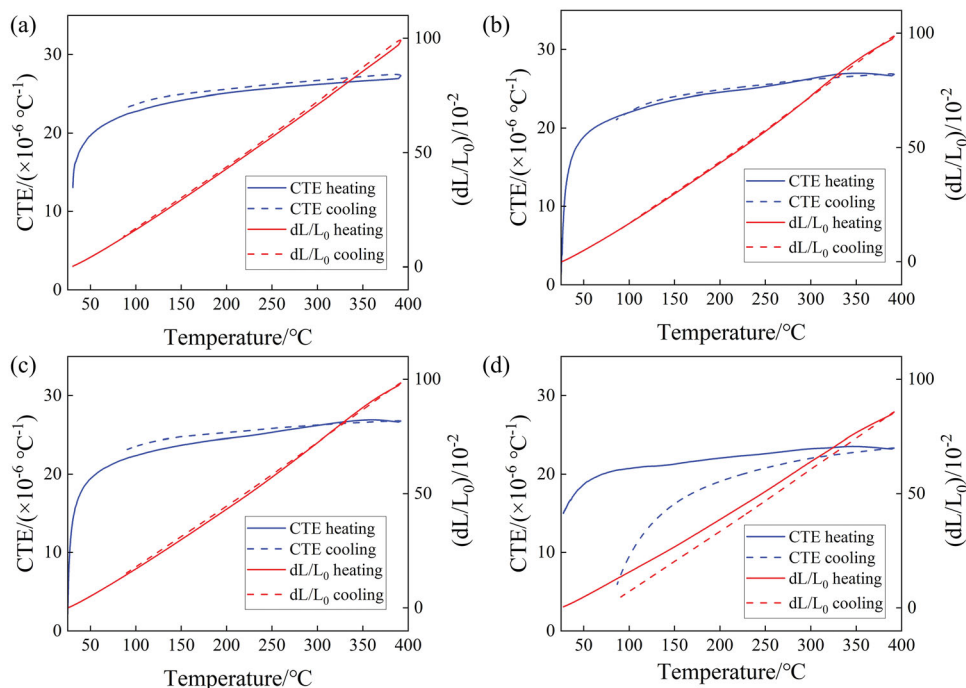
Fig. 7. Thermal expansion curves (red line) and experimental CTE curves (blue line) of (a) Mg/3SiC$_p$, (b) Mg-3Y/1SiC$_p$, (c) Mg-3Y/3SiC$_p$ and (d) Mg-3Y/5SiC$_p$.

The thermal expansion curves and corresponding CTE curves of the Mg/3SiC$_p$ and the Mg-3Y/xSiC$_p$ (x = 1, 3, 5 wt.%) are shown in Fig. 7 with the calculated CTE α also listed in Table III. Compared with pure Mg in Section "Microstructure and Thermal Expansion Behavior of the SiCp Reinforced Composites," the CTE decreased from 27.9×10^{-6}/°C to 27.4×10^{-6}/°C with 3 wt.% SiC particulates. Moreover, the CTE for the Mg-3Y/1SiC, Mg-3Y/3SiC and Mg-3Y/5SiC composites decreased from 27.8×10^{-6}/°C for the Mg-3Y alloy to 26.8×10^{-6}/°C, 26.6×10^{-6}/°C and 23.3×10^{-6}/°C, respectively. With 5 wt.% SiC particulates, the CTE almost matched well with that of Al alloy (23.32×10^{-6}/°C).[5] It seemed that the SiC particulates had a more significant effect on reducing the CTE of the extruded Mg-3Y alloy compared to pure Mg. In addition, with the increasing number of SiC particulates, the thermal expansion coefficient of the composite decreased continuously.

DISCUSSION

Effect of Second Phase on the Thermal Expansion Behavior of Mg Alloys

Compared to the CTE of Mg of 27.9×10^{-6}/°C, the CTEs of Mg-3Sm, Mg-3Nd, Mg-3Gd and Mg-3Y alloys were 27.3×10^{-6}/°C, 27.0×10^{-6}/°C, 27.2×10^{-6}/°C and 27.8×10^{-6}/°C, respectively. It indicated that adding RE elements could marginally decrease the CTE of Mg and improve its dimensional stability. In Fig. 4, there was a gap between the heating and cooling curves. This was because after the heating process, some reduction of the sample length occurred because of the release of the residual strain from the manufacturing of the alloy.[28]

For the different CTEs of Mg-3Sm, Mg-3Nd, Mg-3Gd and Mg-3Y, the main reason was the difference in the volume fraction of the second phases in these alloys. The Mg-3Nd alloy demonstrated the highest volume fraction of the second phase of 6.9% and the

lowest CTE of $27.0 \times 10^{-6}/°C$ among these four alloys. It was because even though similar amount of RE was added to the alloys, Sm, Nd, Gd and Y had very different solubility of 5.8 wt.%, 3.6 wt.%, 23.8 wt.% and 12.0 wt.% in Mg, respectively.[29,30] Among these four RE elements, Nd had the smallest solubility and led to the largest volume fraction of the RE-containing second phase in the alloy. Besides, these second phases normally have a lower CTE and much higher elastic modulus compared to Mg, leading to a strong constraint effect during the thermal expansion of the matrix. The larger volume fraction of the second phase means more interface area between the matrix and the second phases as well, so that the hindering effect was enhanced.[31] Moreover, more second phases also meant the lower the volume fraction of the Mg matrix. The expansion of the alloy was mainly due to the expansion of the matrix, and thus the decrease of the matrix volume fraction would lead to the decrease of the overall CTE of the alloy. This was the reason why the CTE of the alloy decreased gradually with the increasing volume fraction of the second phase. Hassan et al. and Rudjevova et al.[6,28] also reported a similar effect of the Mg_2Cu phase and Mg_2Si phase in the Mg-Cu and AS series alloys, respectively, on decreasing the CTE of Mg alloys.

Effect of SiC_p on the Thermal Expansion Behavior of the Mg-3Y Alloy

As for the composite materials, according to Table III, the presence of the SiC particulates as reinforcement resulted in better dimensional stability compared with the pure Mg and the Mg-Y alloy. The decrease of CTE of Mg/3SiC was marginal compared to pure Mg; this was probably due to the relatively poor distribution of the SiC particulates in this composite.[32] The thermal expansion coefficient of the Mg-3Y/xSiC$_p$ composites decreased with the increasing number of the SiC particulates. When adding 5 wt.% SiC$_p$, the CTE of the composite decreased to $23.3 \times 10^{-6}/°C$. The decreased CTE of the composites could be attributed to the lower CTE of SiC$_p$ ($4.0 \times 10^{-6}/°C$) compared to Mg, good interfacial integrity between reinforcements and the matrix and the ability of the reinforcements to effectively constrain the expansion of the matrix.[24]

In Fig. 7b, c and d, the thermal expansion coefficient of the Mg-3Y/SiC$_p$ composites reached a peak value at about 350°C. During the heating process, thermal expansion occurred for both the SiC particulates and the matrix. Due to the large difference of the CTE between the matrix and the reinforcement, internal thermal stresses localized near the interface. With increasing number of the SiC particulates, there was larger internal thermal stress and more interface. Meanwhile, with increasing temperature, the yield stress of the matrix decreased. At high temperatures, the internal thermal stresses at the interface might achieve or even

exceed the yield stress of the Mg alloy matrix. Thus, plastic deformation of the matrix occurred. In this study, the CTE the Mg-3Y/SiC$_p$ composites started to decrease at above 350°C. Once the composite had undergone plastic deformation during the heating cycle, only the elastic deformation would recover during the cooling cycle with the plastic deformation remained.[33] This leads to the gap between the heating and the cooling curve of CTE. Chen et al.[34] also reported similar phenomena in the Al/SiCp composite. The more SiC particulates in the composites, the more obvious this effect, and the larger the gap between the heating and the cooling curve of CTE. This explained the largest discrepancy between the heating and the cooling curves of Mg-3Y/5SiC$_p$ shown in Fig. 7d among the three Mg-3Y/SiC$_p$ composites.

To better understand the effect of SiC particulates on the thermal expansion behavior of Mg-3Y, three models were employed to compare with the measured CTE for the Mg-3Y/xSiC$_p$ (x = 1, 3, 5 wt.%) composites:

(a) Rule of Mixture (ROM)[35]

According to the ROM, the thermal expansion of the composite consisted of the contributions from both the matrix and the reinforcing particulates based on their volume fractions. It served as the first-order approximation to the overall calculation of the CTE of the composites as follows:

$$\alpha_C = \alpha_m V_m + \alpha_p V_p \tag{2}$$

(b) Turner Model[36]

In this model, assuming that the phases in the composite material only bore hydrostatic pressure without considering the influence of shear stress, and the matrix was uniformly plastically deformed. The CTE of the composite material can be expressed as:

$$\alpha_c = \frac{\alpha_m V_m K_m + \alpha_p V_p K_p}{V_m K_m + V_p K_p} \tag{3}$$

(c) Kerner Model[37]

This model was an improvement on the Turner model. It not only considered the hydrostatic pressure of the phases but also took the influence of shear stress into account. The CTE of the composite material was calculated as:

$$\alpha_c = \alpha_m - (\alpha_m - \alpha_p) \times \frac{K_p(3K_m + 4G_m)V_p}{K_m(3K_p + 4G_m) + 4(K_p - K_m)G_m V_p} \# \tag{4}$$

where a was the coefficient of thermal expansion ($10^{-6}/°C$); V was the volume fraction (%); K was the bulk modulus (GPa); G was the shear modulus

(GPa). The subscripts c, m and p represented the composite, matrix and particulates, respectively. The CTE of the SiC particulates, pure Mg and the Mg-3Y alloy is $4.0 \times 10^{-6}/°C$, $27.9 \times 10^{-6}/°C$ and $27.8 \times 10^{-6}/°C$, respectively. The bulk modulus K of the SiC particulate and the Mg matrix are 400 GPa and 45 GPa, respectively. The shear modulus G of the extruded Mg is 15.4 GPa.[38]

The predicted CTE values of the above three models are listed in Table IV and plotted in Fig. 8 together with the experimental results. It was found that the experimental CTE values of the Mg-3Y/xSiCp (x = 1, 3, 5%) composites were between the predictions of ROM and the Turner model.

The predictability of the three models was further evaluated by the correlation coefficient (R) and the average absolute relative error (AARE), which are defined as:[39,40]

$$R = \frac{\sum_{i=1}^{n}(E_i - \overline{E})(P_i - \overline{P})}{\sqrt{\sum_{i=1}^{n}(E_i - \overline{E})^2 \sum_{i=1}^{n}(P_i - \overline{P})^2}} \quad (5)$$

$$\text{AARE} = \frac{1}{n}\sum_{i=1}^{n}\left|\frac{E_i - P_i}{E_i}\right| \times 100\% \quad (6)$$

where n is 3, E_i is the experimental CTE value and $\overline{E}$ is the mean value of E_i; P_i is the predicted CTE value and $\overline{P}$ is the mean value of P_i. The calculated R and AARE of the three models are summarized in Table V.

The R represents the linear relationship between the experimental and predicted values. The AARE is computed through a term-by-term comparison of the relative error.[41] Among the three models, even though the relative error is slightly higher, the predictions of the Kerner model show a better correlation with the experimental results. The slightly lower experimental CTE values, compared with theoretical Kerner model predictions, were primarily attributed to the promotion effect of the SiC particulates on the precipitation of the $Mg_{24}Y_5$ phase. There was about 0.07% $Mg_{24}Y_5$ phase in the Mg-3Y alloy. However, the volume fractions of $Mg_{24}Y_5$ in the Mg-3Y/1SiC$_p$, Mg-3Y/3SiC$_p$ and Mg-3Y/5SiC$_p$ composites were about 1.62%, 1.73% and 2.22%, respectively. In Fig. 6. the $Mg_{24}Y_5$ phase and the SiC particulates distributed together in strips along the ED. During the solidification of the composite material, the SiC$_p$ reinforcement could work as nuclei and accelerated the precipitation of

$Mg_{24}Y_5$ phase. It was reported that with the addition of SiC$_p$, the reaction enthalpies of both the GP zone and intermetallic phase of Al_2CuMg in the cast SiC$_p$/2024 Al composite were substantially decreased.[42] In addition, according to Section "Effect of Second Phase on the Thermal Expansion Behavior of Mg Alloys," more RE-containing second phases led to a reduced CTE of the material. Therefore, the promotion for the precipitation of the $Mg_{24}Y_5$ phase by the SiC particulates contributed to the lower experimental CTE compared with the model prediction. Besides, the lower experimental CTE values can also be attributed to the coupled effect of the uniform distribution of the SiC particulates with lower CTE and the good interfacial integrity between SiC$_p$ reinforcement and alloy matrix.[43] Hong et al.[26] investigated the thermal expansion behavior of the AZ91/SiC$_p$ composite processed by liquid pressing (the size of the SiC particulates was approximately 10 μm). The
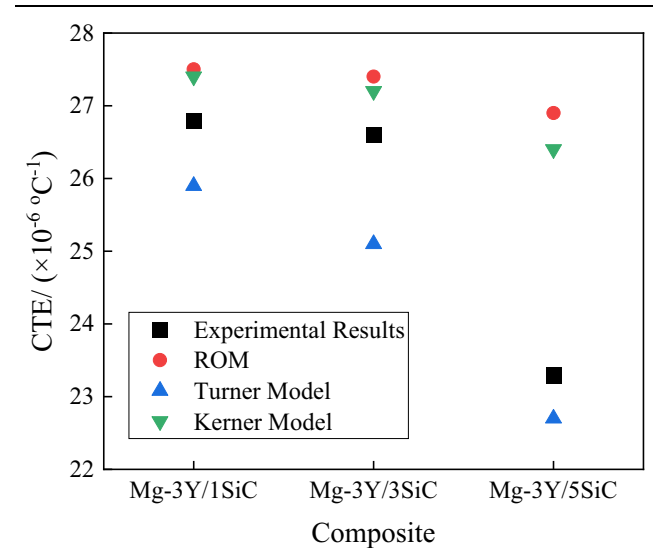

Fig. 8. Predicted and experimental CTE values of the Mg-3Y/xSiCp (x = 1, 3, 5%) composites.

Table V. R and AARE of the three models

	ROM	Turner model	Kerner model
R	0.9903	0.9817	0.9945
AARE	0.0702	0.0386	0.0593

Table IV. Predicted and experimental CTE of the Mg-3Y/SiC$_p$ composites ($\times 10^{-6}/°C$)

Composite	ROM	Turner model	Kerner model	Experimental results
Mg-3Y/1SiC	27.5	25.9	27.4	26.8
Mg-3Y/3SiC	27.4	25.1	27.2	26.6
Mg-3Y/5SiC	26.9	22.7	26.4	23.3

measured CTE was also closer to the prediction of the Kerner model than other models.

CONCLUSION

This work investigated the thermal expansion behavior of the extruded Mg-3Sm, Mg-3Nd, Mg-3Gd, and Mg-3Y alloys and the extruded Mg-3Y/xSiC$_p$ (x = 1, 3 and 5 wt.%) composites. The following conclusions can be drawn:

(1) Adding 3 wt.% RE elements could marginally decrease the CTE of Mg and improve the dimensional stability through the formation of RE-containing second phases. The CTEs of pure Mg, Mg-3Sm, Mg-3Nd, Mg-3Gd and Mg-3Y alloys were about $27.9 \times 10^{-6}/°C$, $27.3 \times 10^{-6}/°C$, $27.0 \times 10^{-6}/°C$, $27.2 \times 10^{-6}/°C$ and $27.8 \times 10^{-6}/°C$, respectively. The lowest CTE of Mg-3Nd was attributed to the smallest solubility of Nd in Mg, which led to the largest volume fraction of the RE-containing second phase in the alloy.

(2) Adding SiC particulates could significantly reduce the CTE of the composite. With the increasing volume fraction of SiC$_p$, the CTE of the Mg-3Y/xSiC$_p$ composites continuously decreased. The CTEs of Mg/3SiC, Mg-3Y/1SiC, Mg-3Y/3SiC and Mg-3Y/5SiC were about $27.4 \times 10^{-6}/°C$, $26.8 \times 10^{-6}/°C$, $26.6 \times 10^{-6}/°C$ and $23.3 \times 10^{-6}/°C$, respectively. The decreased CTE of the composites was due to the low CTE of SiC$_p$, good interfacial integrity between reinforcements and the matrix and the ability of the reinforcements to effectively constrain the expansion of the matrix.

(3) Adding SiC particulates promoted the precipitation of Mg$_{24}$Y$_5$ phase in the extruded Mg-3Y/xSiC$_p$ composites. There was about 0.07% Mg$_{24}$Y$_5$ phase in the extruded Mg-3Y alloy. The volume fractions of Mg$_{24}$Y$_5$ phase in the Mg-3Y/1SiC$_p$, Mg-3Y/3SiC$_p$ and Mg-3Y/5SiC$_p$ composites were about 1.62%, 1.73% and 2.22%, respectively. The CTE of the Mg-3Y/xSiC$_p$ composites reached a peak value at about 350°C.

(4) Rule of mixture, the Turner model and the Kerner model were utilized to predict the CTE of the Mg-3Y/SiC$_p$ composites. The predictions of the Kerner model show a better correlation with the experimental results. The slightly lower experimental CTE compared with the predicted values of the Kerner model was primarily attributed to the promotion effect of the SiC particulates on the precipitation of the Mg$_{24}$Y$_5$ phase.

AUTHOR CONTRIBUTIONS

Tong Wang: Conceptualization, Writing-original draft, Funding acquisition. Chaoqi Feng: Investigation. Can Wang: Data curation. Ruizhen Guo: Methodology. Wenyi Hu: Investigation. Dabiao Xia: Formal analysis. Qichi Le: Supervision. Manoj Gupta: Writing-review & editing, Supervision.

DATA AVAILABILITY

The raw/processed data are available from the corresponding author upon reasonable request.

CONFLICT OF INTEREST

The authors declare that they have no known competing financial interests or personal relationships that could have appeared to influence the work reported in this paper.

REFERENCES

1. L. Liu, X. Chen, and F. Pan, *J. Magn. Alloys* 9, 1906 https://doi.org/10.1016/j.jma.2021.10.001 (2021).
2. W.A. Monteiro, *Light Met. Alloys Appl.* 12, 229 (2014).
3. M. Gupta and S.N.M. Ling, *Magnesium, Magnesium Alloys, and Magnesium Composites* (Wiley, Hoboken, 2011).
4. E.A. Brandes and G. Brook, *Smithells Metals Reference Book* (Elsevier, Amsterdam, 2013).
5. S. Wu, D. Zhou, Y. Huang, K. Wang, J. Song, Z. Dong, and B. Jiang, *Scr. Mater.* 214, 114680 https://doi.org/10.1016/j.scriptamat.2022.114680 (2022).
6. S.F. Hassan and M. Gupta, *Met. Sci. J.* 19, 253–259 (2003).
7. T. Guo, S. Wu, X. Zhou, S. Lü, and L. Xia, *Mater. Chem. Phys.* 253, 123260 https://doi.org/10.1016/j.matchemphys.2020.123260 (2020).
8. Q.C. Jiang, H.Y. Wang, Y. Wang, B.X. Ma, and J.G. Wang, *Mater. Sci. Eng. A* 392, 130 https://doi.org/10.1016/j.msea.2004.09.007 (2005).
9. N. Yasuda and S. Kimura, *Mater. Trans.* 57, 1010 https://doi.org/10.2320/matertrans.M2016078 (2016).
10. N. Rahulan, S. Gopalan, and S. Kumaran, *Mater. Today Proc.* 5, 17935 https://doi.org/10.1016/j.matpr.2018.06.123 (2018).
11. F. Barson, S. Legvold, and F.H. Spedding, *Phys. Rev.* 105, 418 (1957).
12. F.H. Spedding, J.J. Hanak, and A.H. Daane, *J. Less-Common Met.* 3(2), 110 (1961).
13. A. Kumar, G.K. Meenashisundaram, V. Manakari, G. Parande, and M. Gupta, *J. Alloys Compd.* 695, 3612 https://doi.org/10.1016/j.jallcom.2016.11.400 (2017).
14. H. Ma, Z. Li, and J. Wang, *Mater. Res. Express* 8, 076518 https://doi.org/10.1088/2053-1591/ac144e (2021).
15. N. Dong, J. Wang, H. Ma, and P. Jin, *Mater. Today Commun.* 29, 102894 https://doi.org/10.1016/j.mtcomm.2021.102894 (2021).
16. H. Ferkel and B.L. Mordike, *Mater. Sci. Eng. A* 298, 193 https://doi.org/10.1016/S0921-5093(00)01283-1 (2001).
17. L.-Y. Chen, J.-Q. Xu, H. Choi, M. Pozuelo, X. Ma, S. Bhowmick, J.-M. Yang, S. Mathaudhu, and X.-C. Li, *Nature* 528, 539 https://doi.org/10.1038/nature16445 (2015).
18. B.W. Chua, L. Lu, and M.O. Lai, *Compos. Struct.* 47, 595 https://doi.org/10.1016/S0263-8223(00)00031-3 (1999).
19. S.K. Thakur, B.K. Dhindaw, N. Hort, and K.U. Kainer, *Metall. Mater. Trans. A* 35, 1167 https://doi.org/10.1007/s11661-004-0043-6 (2004).

20. J.H. Son, W.J. Lee, Y.H. Park, and I.M. Park, *Mech. Compos. Mater.* 47, 427 https://doi.org/10.1007/s11029-011-9220-z (2011).
21. D.H. Cho, J.H. Nam, B.W. Lee, S.O. Yim, and I.M. Park, *Met. Mater. Int.* 22, 332 https://doi.org/10.1007/s12540-016-5454-6 (2016).
22. S. Seetharaman, J. Subramanian, K.S. Tun, A.S. Hamouda, and M. Gupta, *Materials* 6, 1940 (2013).
23. M. Jayamathy, S.V. Kailas, K. Kumar, S. Seshan, and T.S. Srivatsan, *Mater. Sci. Eng. A* 393, 27 https://doi.org/10.1016/j.msea.2004.09.070 (2005).
24. W.L.E. Wong and M. Gupta, *Solid State Phenom.* 111, 91 https://doi.org/10.4028/www.scientific.net/SSP.111.91 (2006).
25. S.K. Thakur, G.T. Kwee, and M. Gupta, *J. Mater. Sci.* 42, 10040 https://doi.org/10.1007/s10853-007-2004-0 (2007).
26. S.J. Hong, S.-B. Lee, H.B. Kim, J. Kim and S.-K. Lee, in *18th International Conference on Composite Materials* (2011).
27. K.-C. Shen, G.-H. Li, and W.-M. Wang, *Trans. Nonferrous Met. Soc. China* 26, 2900 https://doi.org/10.1016/S1003-6326(16)64419-9 (2016).
28. A. Rudajevová and P. Lukáč, *Mater. Sci. Eng. A* 397, 16 https://doi.org/10.1016/j.msea.2004.12.036 (2005).
29. L.L. Rokhlin, *Magnesium Alloys Containing Rare Earth Metals-Structure and Properties* (Taylor & Francis Inc., New York, 2003).
30. M. Hampl, C. Blawert, M.R. Silva Campos, N. Hort, Q. Peng, K.U. Kainer, and R. Schmid-Fetzer, *J. Alloys Compd.* 581, 166 https://doi.org/10.1016/j.jallcom.2013.07.042 (2013).
31. T. Guo, S. Wu, X. Zhou, S. Lu, and L. Xia, *Mater. Chem. Phys.* https://doi.org/10.1016/j.matchemphys.2020.123260 (2020).
32. K.S. Tun and M. Gupta, *Compos. Sci. Technol.* 67, 2657 https://doi.org/10.1016/j.compscitech.2007.03.006 (2007).
33. P. Lukac and A. Rudajevová, *Kovove Materialy* 41, 281–292 (2003).
34. N. Chen, H. Zhang, M. Gu, and Y. Jin, *J. Mater. Process. Technol.* 209, 1471 https://doi.org/10.1016/j.jmatprotec.2008.03.054 (2009).
35. J.K. Chen, and I.S. Huang, *Compos. Part B Eng.* 44, 698 https://doi.org/10.1016/j.compositesb.2012.01.083 (2013).
36. P.S. Turner, *J. Res. Natl. Bur. Stand.* 37, 239 https://doi.org/10.6028/jres.037.015 (1946).
37. E.H. Kerner, *Proc. Phys. Soc. Sect. B* 69, 808 https://doi.org/10.1088/0370-1301/69/8/305 (1956).
38. H. Watanabe, J. Tani, H. Kido, and K. Mizuuchi, *Mater. Sci. Eng. A* 494, 291 https://doi.org/10.1016/j.msea.2008.04.037 (2008).
39. X. Xiao, G.Q. Liu, B.F. Hu, X. Zheng, L.N. Wang, S.J. Chen, and A. Ullah, *Comput. Mater. Sci.* 62, 227 https://doi.org/10.1016/j.commatsci.2012.05.053 (2012).
40. T. Wang, Y. Chen, B. Ouyang, X. Zhou, J. Hu, and Q. Le, *Mater. Sci. Eng. A* 816, 141259 https://doi.org/10.1016/j.msea.2021.141259 (2021).
41. H.-Y. Li, D.-D. Wei, Y.-H. Li, and X.-F. Wang, *Mater. Des.* 35, 557 https://doi.org/10.1016/j.matdes.2011.08.049 (2012).
42. J. Lin, P. Li, and R. Wu, *Acta Metall. Sin.* 28(10), 85 (1992).
43. S.F. Hassan and M. Gupta, *Mater. Sci. Technol.* 20, 1383 https://doi.org/10.1179/026708304X3980 (2004).